Short Communication

Synthesis and First-principle Calculation of TiO$_2$ Rutile Nanowire Electrodes for Dye-sensitized Solar Cells

Jinghua Hu[1,†] , Peihan Liu[1,†] , Mengwei Chen[1], Sa Li[2], Yingping Yang[1,*]

[1]School of Science, Wuhan University of Technology, Wuhan 430070,China
[2]KTH Royal Institute of Technology, Department of Material Science & Engineering, SE-10044 Stockholm, Sweden
† Jinghua Hu, Peihan Liu have been contributed equally to this work
[*]E-Mail: ypyang@whut.edu.cn

In this paper, a TiO$_2$ nanowire film synthesized via a hydrothermal method was prepared as a photoanode for dye-sensitized solar cells (DSSCs). The synthesized TiO$_2$ nanowires were characterized by transmission electron microscopy and X-ray diffraction. The TiO$_2$ nanowire film greatly improved the efficiency of the DSSC owing to the rapid interfacial electron transport in the one-dimensional TiO$_2$ nanowires. The light absorption and interfacial electron transport, which play important roles in the efficiency of DSSCs, were investigated by UV-vis absorption spectroscopy and electrochemical impedance spectroscopy. The energy band structure and electron density of states of the rutile nanowire were calculated using a first-principles method and compared to bulk anatase and rutile TiO$_2$ phases. The band gap of the rutile TiO$_2$ nanowire was found to be less than that of anatase TiO$_2$ by 0.6 eV. Further calculations using GGA+U yielded a similar band gap reduction. In addition to the redshift of the absorption edge originating from the smaller band gap, the larger surface area of the TiO$_2$ nanowire compared to the bulk material is expected to facilitate the migration of photogenerated electrons and holes from inside to the surface of the material. This would result in a considerable improvement of the photocatalytic efficiency of TiO$_2$.

1. INTRODUCTION

Dye-sensitized solar cells (DSSCs) have attracted a great deal of interest due to their low cost, broad source, relatively easy design, low energy consumption and suitability for extensive production. Typically, DSSCs consist of transparent conductive optical glass, a photoanode, a dye, electrolyte and the electrode. The photoanode plays an important role in determining the performance of DSSCs,

which usually use TiO_2, ZnO, SnO_2, Fe_2O_3, CdS, WO_3, Ta_2O_3, In_2O_3, $SrTiO_3$, etc. [1-3]. Among them, TiO_2 is one of the most promising candidates because of its outstanding properties, such as its light absorption capabilities, chemical inertness and stability [4].

Since 1991, TiO_2 nanoparticle photoanodes (NPPs) have been widely used to assemble dye-sensitized solar cells. Thus far, this NPP has always been considered a model of a porous anode. However, the NPP structure is not just ideal due to its low electronic transmission efficiency, low surface area and weak scattering of visible/ infrared light [5]. To improve the efficiency of DSSCs, one-dimensional (1-D) nanomaterials, such as nanowires [6-8], nanotubes [9-14], and nanofibers [15], have been synthesized by different methods, such as sol-gel synthesis, template synthesis, anodic oxidation and hydrothermal synthesis [16-20]. Nanowire is a typical one-dimensional material. It is reported that TiO_2 powders crystallized by the solvothermal reaction in methanol possessed excellent photocatalytic activity and thermal stability[6]. TiO_2 exhibiting S-peaks is a promising charge storage material[7]. TiO_2 anatase nanowires were synthesized by the hydrothermal processing. At 900 ^oC, they transformed from anatase structure into rod-shaped rutile grains[8].

In this paper, we synthesized a TiO_2 nanowire film via a hydrothermal method and used it as a photoanode to assemble a DSSC. The structural and photoelectrochemical properties of the TiO_2 nanowire electrode and DSSC were characterized using X-ray diffraction (XRD), UV-visible absorption spectra, transmission electron microscopy (TEM), photocurrent-voltage curves and EIS analyses.

2. EXPERIMENTAL

2.1. Materials

Commercial TiO_2 nanoparticles (P25, from Degussa) were used as received. Cis-bis(isothiocyanato)bis(2,2′-bipyridyl-4,4′-dicarboxylato)ruthenium(II) bis-tetrabutylammonium (N719) was purchased from Dyesol. Acetonitrile was purchased from Alfa Aesar. LiI, I_2 and tert-butylpyridine were purchased from Aldrich. 1-Propyl-3-methylimidazolium iodide was purchased from J&K. All the reagents were used without any further pretreatment. All solutions were prepared with distilled water. FTO (sheet resistance, 14-20 Ω/cm^2) was purchased from Hartford Glass Co. It was used as substrates for further experiments and pretreated by rinsing in an ultrasonic bath of detergent and acetone for 10 and 20 min respectively, then rinsing with a large amount of deionized water and ethanol and finally drying at 80 °C .

2.2. Preparation of the TiO_2 nanowire powder

TiO_2 nanowires were synthesized via a hydrothermal method without the addition of any templates or surfactants. Titanium (IV) isopropoxide (TTIP (97%), Aldrich Chemicals) was dropped into 10 M hydrochloric acid (HCl (35%), Aldrich Chemicals) with constant stirring at 25 °C and then kept constant for 1 h. The hydrothermal reaction process in 10 M HCl was carried out at 180 °C for 24

h. After the hydrothermal process, the resulting precipitates was cooled to room temperature and washed several times with ethanol and distilled water. After drying in an oven at 50 °C , the TiO_2 nanowire powders was obtained. The nanowire powder was annealed at 900 °C and then is naturally cooled.

2.3. Preparation of the TiO_2 nanowire/FTO glass and P25/FTO glass photoanode

To compare the photoelectrochemical properties of the TiO_2 nanowire structure as a working electrode, solar cells were fabricated by a conventional method. The TiO_2 nanowire powder and P25 powder were pasted on F-doped SnO_2 (FTO) coated glass using a doctor-blade method, followed by sintering at 500 °C for 1 h in air, resulting in 30 μm thick films.

2.4. Fabrication of the dye-sensitized solar cells

A P25/TNT array/FTO glass photoanode and a the TNT array/FTO glass photoanode were immersed into a 0.3 mM/L anhydrous solution of N719 and kept at room temperature for 24 h to ensure maximum sensitizer uptake. The dye-sensitized photoanodes were separated by scotch tape spacers. A solar cell with a sandwich structure was assembled by placing Pt-coated FTO conducting glass on the photoanode. The assembled cell was then clipped together for later tests. The electrolytes (0.3 M LiI, 0.05 M I_2, 0.6 M 1-propyl-3-methylimidazolium iodide and 0.5 M tert-butylpyridine in dry acetonitrile) were injected into the open cell from the edge, capillary forces attracted a thin layer of electrolyte into the inter-electrode space, and the cell was tested immediately.

2.5. Measurements

We used X-ray powder diffraction (XRD, MAX-RB RU-200B, Japan) to characterize the samples crystalline phase purity. Transmission electron microscopy (TEM, JEM-2100F, Japan) was used to measure the morphologies and sizes of the samples. Diffuse reflectance spectra and the surface concentration of N719 of the samples were measured by a UV-visible spectrophotometer (UV3600, Shimadzu, Japan). The current-voltage (I-V) characteristics were measured under AM 1.5G illumination at a 100 mW cm^{-2} intensity provided by a solar light simulator (Oriel Sol3A, Newport Corporation, USA). Electrochemical impedance spectroscopy (EIS) was measured by an electrochemical workstation (IM6, Germany) under the same simulated conditions. The testing cell had an active area of 0.16 cm^2, and EIS had a frequency range from 0.1 Hz to 100 kHz.

3. RESULTS AND DISCUSSION

3.1. XRD

The crystalline phase and the grain size of TiO_2 have a great impact on the efficiency of photoelectric conversion of the dye-sensitized solar cell. We used X-ray diffraction (XRD) to characterize the phase structure of the TNA TiO_2 nanowires. Figure 1 shows the XRD patterns of the

TiO_2 nanowires annealed at 900 °C. The XRD data show that an anatase crystalline phase with a very small amount of rutile phase is formed after annealing at 900°C, and the crystal growth is sufficient. The peak of the (101) crystal plane is higher than those of the other crystal planes, and this shows that the TiO_2 nanowires preferentially grew along the (101) crystal plane.
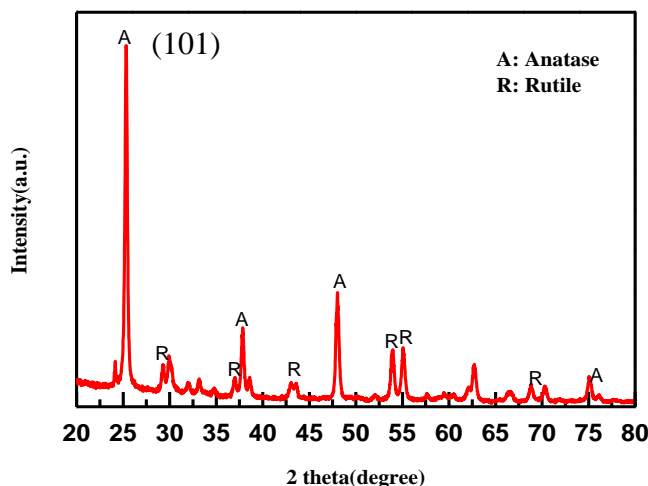
Figure 1. XRD patterns of the TiO_2 nanowires annealed at 900 ℃.

3.2. UV-visible absorption spectra

UV-visible absorption spectra are shown in Figure 2 for the annealed sample. The spectra of the TiO_2 nanowire film presented an absorption edge at approximately 380 nm, which corresponds to a band gap of 3.27 eV. It's reported that the anatase TiO_2 has a band gap of 3.2eV[21] similar to the result of our experiment. The narrow band gap improves the electron transfer capability from the valance band to the conduction band and prevents photoinduced electrons in the conduction band of TiO_2 from returning to the dye molecules or electrolyte for recombination.
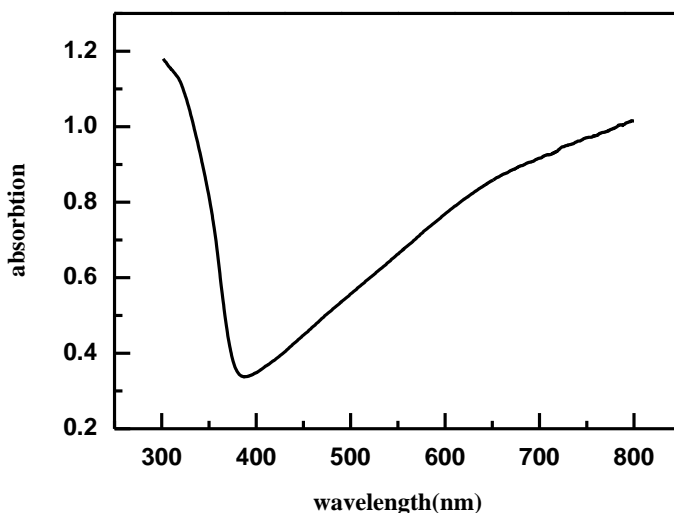
Figure 2. Absorption spectra of the nanowire film.
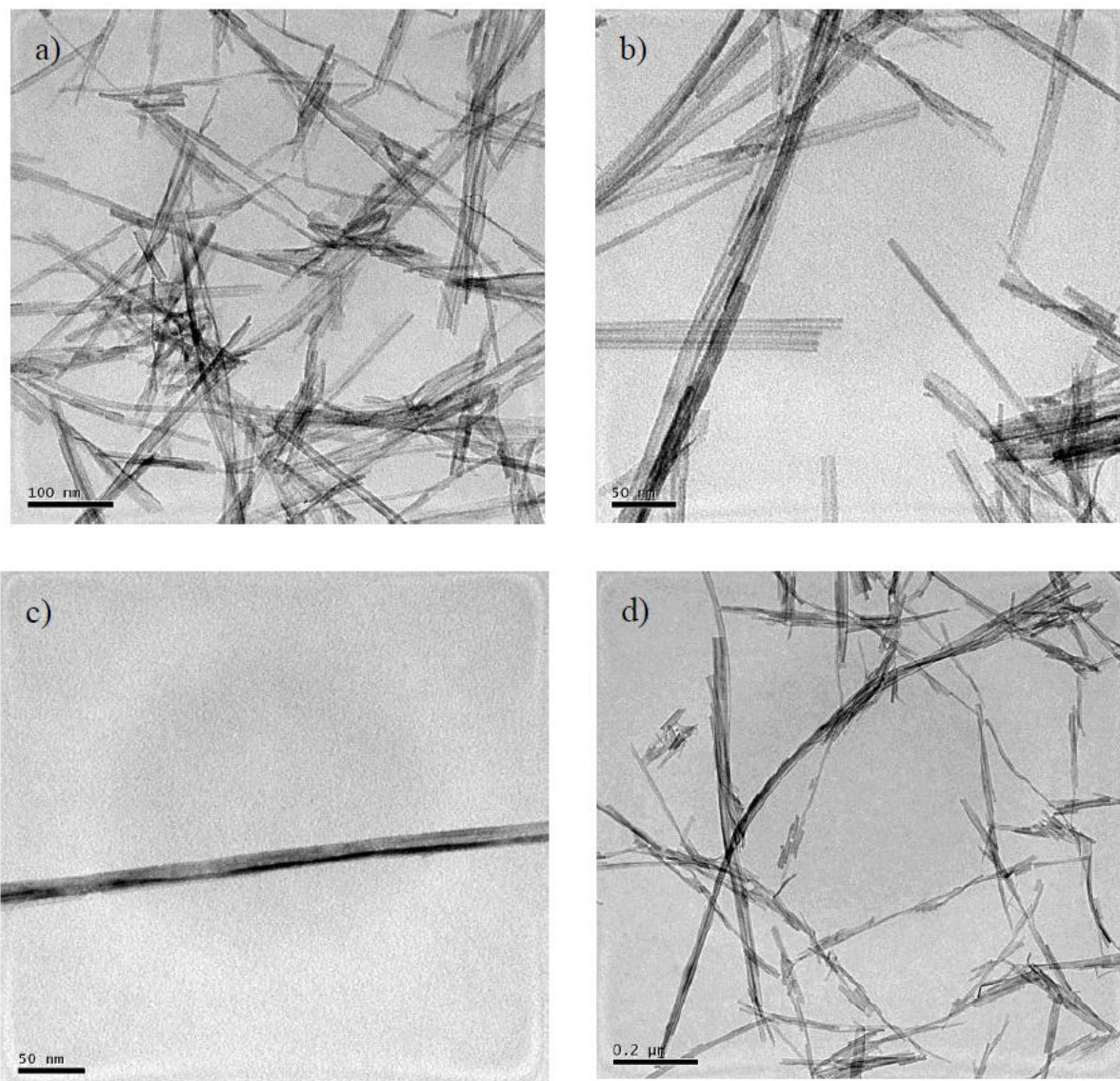
3.3. TEM

Figure 3. Transmission electron microscopy(TEM) images of the TiO_2 electrodes.(a)scaleplate of 100 nm;(b)scaleplate of 50 nm;(c)a separate nanaowire under the scaleplate of 50 nm;(d)scaleplate of 0.2 μm

Figure 3 shows the TEM images of the TiO_2 nanowire film obtained by means of the hydrothermal method. The sample was composed of fine nanowires. Figure 3(a) and (d) show that the synthesized TiO_2 nanowires are composed of uneven crisscrossed wires with lengths of approximately 0.6 μm to 2 μm. It is understood from Figure 3(b) and (c) that the nanowires possess an average diameter of 10 nm with very smooth surfaces. TiO_2 nanowires with high a specific surface area are advantageous to dye adsorption and have a certain advantage in electronic transmission.

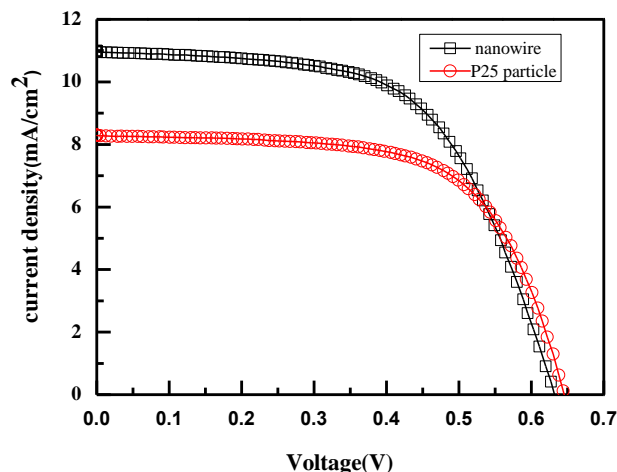*3.4. Photovoltaic performances of the DSSCs*

Figure 4. Photocurrent-voltage curves measured using the TiO_2 nanowires as a photoelectrode compared to P25 particles as a photoelectrode.

To evaluate the performance of the dye-sensitized solar cells using the TiO_2 nanostructures, as shown in Figure 4, photocurrent-voltage curves were obtained using the TiO_2 nanowires as a photoelectrode, which were compared to the use of P25 particles as a photoanode (Table1). The open-circuit voltages (V_{oc}) of the TiO_2 nanowires and P25 particles are similar. The short-circuit current density (J_{sc}), fill-factor (FF) and cell efficiency (η) of the TiO_2 nanowires are 8.24 mAcm^{-2}, 0.59 and 4.04%, respectively, while those of the P25 particles are 10.91 mAcm^{-2}, 0.59 and 3.14%. The short-circuit current density, cell efficiency and fill-factor of the TiO_2 nanowires are higher than those of the P25 particles. DSSC based on the self-branched TiO_2 nanowires also shows a significant improvement compared to that of P25 TiO_2 in Li's paper[22]. It could be concluded that compared to the P25 particles, the TiO_2 nanowires show excellent cell performance.

Table 1. Comparison of the photovoltaic performances of DSSCs made from the nanowire film and P25 film

	Jsc (mA cm^{-2})	Voc (V)	FF	H(%)
Nanowire	10.91	0.63	0.59	4.04
P25	8.24	0.64	0.59	3.14

3.5. EIS analyses

To gain further insight into the inner working processes of the solar cells, electrochemical impedance spectroscopy (EIS) was performed in the dark and under illumination with an electrochemical workstation and simulated using an equivalent circuit. The Nyquist plots of the DSSCs using the TiO_2 nanostructures are shown in Figure 5. Figure 5(a) shows two semicircles, indicating that the TiO_2 nanowire film delivers a better DSSC performance having a smaller resistance value. The

electron lifetime can be calculated from the frequency peak in the low frequency($\tau_e = 1/2\pi f_{max}$) of Figure 5(b)[23]. Then, we can see that TiO$_2$ nanowire film DSSCs obtain longer electron lifetime compared to the P25 nanoparticle film.
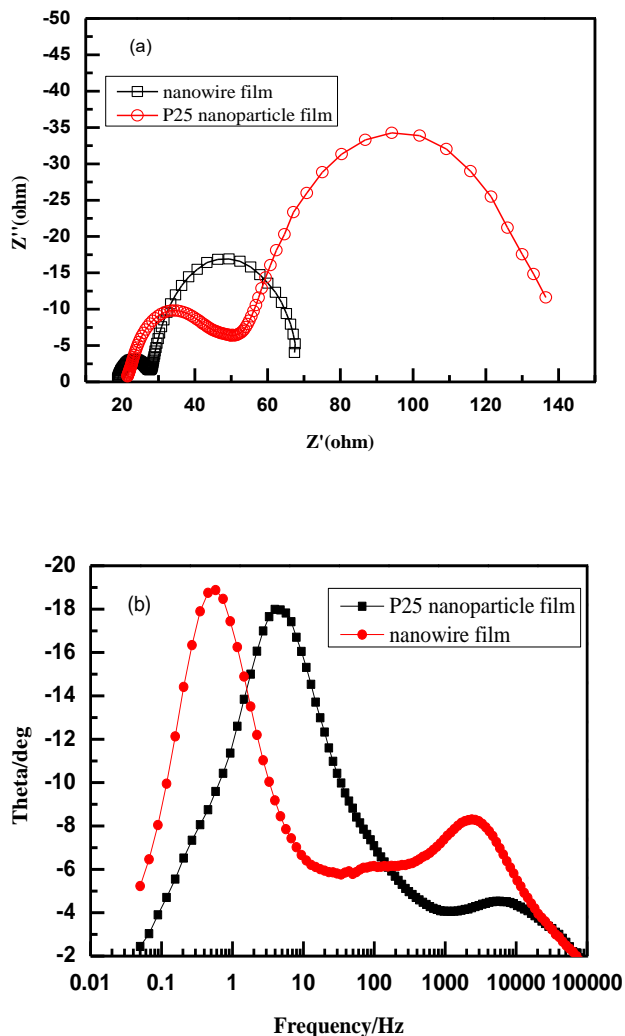
Figure 5. (a) Nyquist plots of the DSSCs; **(b)** Bode phase diagrams of the DSSCs

4. THEORY

4.1. Methods

A square-shaped TiO$_2$ nanowire with a length of 13 Å was generated from a bulk rutile TiO$_2$ supercell (12x12x2). The nanowire supercell consists of 150 atoms and has a vacuum space of approximately 37 Å along the [100] and [010] directions to its periodic images. The nanowire has infinite length along the [001] direction, as shown in Figure 6. The relaxation of the nanowire and its electronic structure were calculated using the Vienna ab initio simulation package (VASP)[24] and the projector augmented wave (PAW)[25] method. The PAW generalized gradient approximation

(GGA)[26]potentials with the valence states of 3d and 4s for Ti and 2s and 2p for O were used. High precision calculations with a cutoff energy of 400 eV for the plane-wave basis were performed. The atomic coordinates were optimized with the shape and volume of the supercell fixed. For sampling the irreducible wedge of the Brillouin zone, we used k-point grids of 1x1x4 for the rutile nanowire. In all the calculations, self-consistency was achieved with a tolerance in the total energy of at least 0.1 meV. To study the magnetic properties of the TiO_2 nanowire, we carried out spin-polarized calculations. To explore the strong on-site Coulomb repulsion among the localized Ti 3d electrons, GGA+U(Hubbard parameter) calculations with U=3.0 and J(exchange)=0.86 were performed to compare with the GGA results.

4.2. Results and discussion

TiO_2 exists in the anatase phase under ambient conditions and undergoes a transition to the rutile phase at temperatures well in excess of 600 °C[27]. Anatase TiO_2 has a tetragonal structure and belongs to the space group I41/amd (#141). In this structure, each Ti atom is octahedrally bonded to six O atoms with four O atoms lying at a distance of 1.94 Å from Ti, while the other two are at a distance of 1.99 Å. The rutile TiO_2 structure belongs to the space group P42/mnm (#136). In this structure, each Ti is also octahedrally coordinated with O atoms with four of them lying on the (110) plane at a distance of 1.95 Å, while the other two lie along the [110] direction at a distance of 1.98 Å.

First, we discuss the atomic relaxation in the $Ti_{50}O_{100}$ nanowire. The total energy of the relaxed structure is found to be 16.87 eV (0.11 eV/atom) lower than that of the unrelaxed configuration. The Ti atoms on the outermost surface are bonded to either five or six O atoms. The relaxed average Ti-O bond lengths are 1.93 Å and 2.0 Å compared to 1.96 Å in the bulk rutile TiO_2 structure. The relaxed TiO_2 nanowire is nonmagnetic.
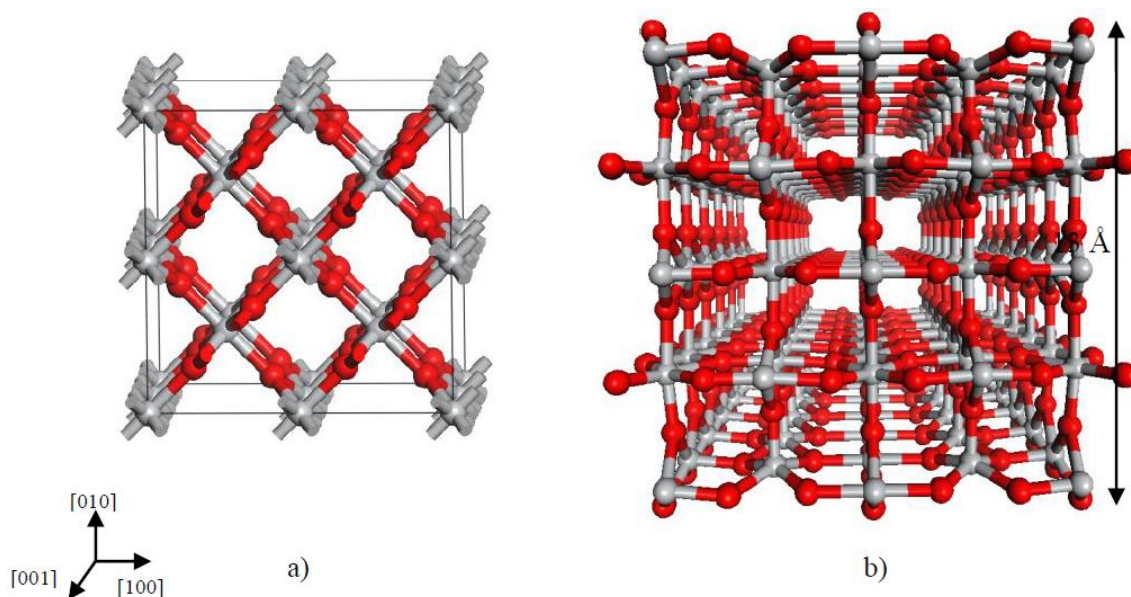

Figure 6. (a) Rutile TiO_2 (2x2x2) supercell structure; **(b)** $Ti_{50}O_{100}$ squared-shaped nanowire, which is infinite along the [001] direction.

We present the density of states (DOS) for anatase TiO_2, rutile TiO_2 and the $Ti_{50}O_{100}$ nanowire in Figure 7. In anatase TiO_2, the lower valence band (LVB) is dominated by O-2s states. The upper valence band (UVB) is composed of O-2p states and Ti-3d states. The UVB is separated from the conduction band (CB) by a band gap of 1.97 eV. The band gap increases to 2.28 eV in the GGA+U calculations. For the rutile phase, the width of the UVB is larger than that of the anatase phase, 5.8 eV versus 5 eV, indicating stronger bonding in the rutile phase. For the $Ti_{50}O_{100}$ nanowire, the GGA calculated band gap is 1.33 eV, which is 0.35 eV less than that in the rutile phase. The GGA+U calculation yields a band gap of 1.65 eV, which is 0.33 eV lower than that the rutile phase. The calculated band gaps for the anatase TiO_2, rutile TiO_2, and the $Ti_{50}O_{100}$ nanowire are given in Table 2.

Table 2. The calculated band gaps for anatase TiO_2, rutile TiO_2 and $Ti_{50}O_{100}$ nanowire.

Systems	GGA	GGA+U	Experiment
Anatase TiO_2 phase	1.97	2.28	3.21[22]
Rutile TiO_2 phase	1.68	1.98	3.0[23]
$Ti_{50}O_{100}$ nanowire	1.33	1.65	

Even though the GGA+U calculations agree better with the experimental band gaps for the anatase and rutile phases, we note that the difference in the band gaps is almost independent of the parameter U.
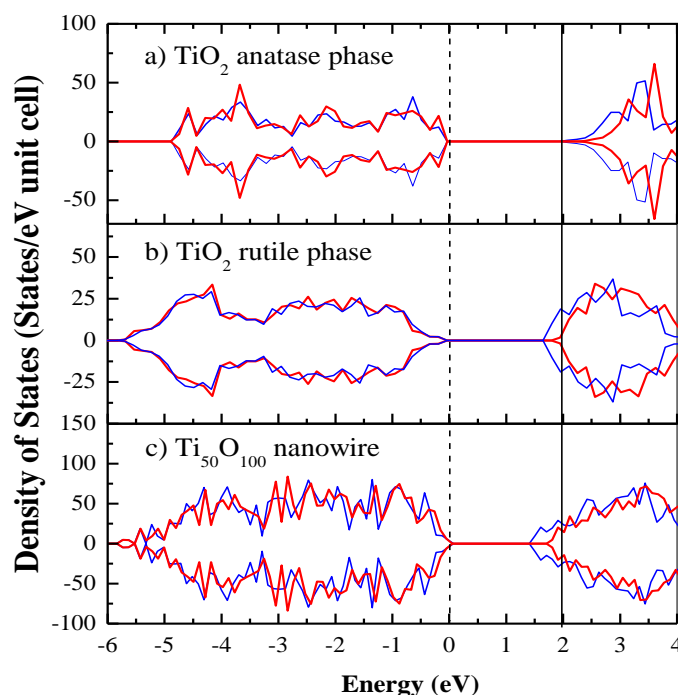

Figure 7. Density of states of **(a)** the anatase TiO_2 phase (2x2x2 supercell), **(b)** the rutile TiO_2 phase (2x2x2 supercell) and **(c)** the $Ti_{50}O_{100}$ nanowire. The GGA and GGA+U calculations are represented by blue and red lines, respectively. The Fermi level is represented by the dashed line, and the bottom of conduction band of the anatase TiO_2 phase is marked by the solid line.

In addition to the redshift of the optical absorption edge, the TiO_2 nanowire has an appreciable surface area relative to bulk TiO_2. Coakley and McGehee suggested that nanostructuring of the donor and acceptor phases to fabricate ordered bulk heterojuction with controlled dimensions could help achieving full exciton harvesting[28]. They chose the mesoporous TiO_2 films because of the pores with a diameter less than 10 nm, and they provide continuous ways for the transmission of electrons. The diameter of the square-shaped TiO_2 is 1.3 nm in our calculations. It is reported that non-equilibrium electrons and holes in most organic semiconductors[29] will recombine when they travel a distance of approximately 5–10 nm. Thus, compared to the bulk materials, the migration of the photoproduced electrons and holes from inside to the surface in our TiO_2 structure will be facilitated in the nanowire.

5. CONCLUSIONS

In summary, a TiO_2 nanowire film was successfully synthesized via a hydrothermal method. The dye-sensitized solar cell assembled by employing these TiO_2 nanowires as an electrode showed excellent performance compared to the use of P25 particles. In the photoelectron chemical analysis, the DSSCs assembled with the TiO_2 nanowire film had a higher short-circuit current density, cell efficiency, and fill-factor and a longer electron lifetime than that with the P25 particles. The experimental results show that the TiO_2 nanowire film could greatly improve the efficiency of DSSCs, owing to the rapid interfacial electron transport in the one-dimensional TiO_2 nanowires.

The theoretical studies show that the band gap of the nanowire is narrowed by approximately 0.6 eV in comparison to anatase TiO_2. The reduction of the band gap will shift the absorption edge of TiO_2 to the visible light region, thus improving its photocatalytic efficiency under visible light. In addition, the small dimension of the nanowire will prevent electrons and holes from recombining.

References

1. A. Birkel, Y.G. Lee, D. Koll, X.V. Meerbeek, S. Frank, M.J. Choi, Y.S. Kang, K. Char and W. Tremel, *Energy Environ Sci.*, 5 (2012) 5392.
2. D.W. Kim, S.S. Shin, I.S. Cho, S. Lee, D.H. Kim, C.W. Lee, H.S. Jung and K.S. Hong, *Nanoscale.*, 4 (2012) 557.
3. H.M. Zhang, Y. Wang, D.J. Yang, Y.B. Li, H.W. Liu, P.Y. Liu, B.J. Wood and H.J. Zhao, *Adv. Mater.*, 24 (2012) 1598.
4. A. Matsuda, S. Sreekantan and W. Krengvirat, *Journal of Asian Ceramic Societies*, 1 (2013) 203.
5. A.I. Hochbaum and P. Yang, *Chem Rev.*, 110 (2010) 527.
6. S. Yin, Y. Fujishiro, J. Wu, M. Akia and T. Sato, *J. Mater. Proc. Tech.*, 137 (2003) 45.
7. L. Kavan, M. Kalbac, M. Zukalova, I. Exnar, V. Lorenaen, R. Nesper and M. Gratzel, *Chem. Mater.*, 16 (2004) 477.

8. R. Yoshida, Y. Suzuki and S. Yoshikawa, *J. Solid State. Chen.*, 178 (2005) 2179.
9. A.F. Kanta, M. Poelman, A. Decroly, *Solar Energy Materials and Solar Cells*, 133 (2015) 76.
10. M.D. Ye, D.J. Zheng, M.Y. Wang, C. Chen, W.M. Liao, C.G. Lin and Z.Q. Lin, *ACS. Appl. Mater. Interfaces*, 6 (2014) 2893.
11. J.H. Hu, S.Q. Tong, Y.P. Yang, J.J. Cheng, L. Zhao, J.X. Duan, *Acta. Metallurgica Sinica.*, 29 (2016) 840.
12. J.H. Hu, J.J. Cheng, S.Q. Tong, Y.P. Yang, M.W. Chen, S.W. Hu, *International Journal of Photoenergy*, 2016, Available online:http://dx.doi.org/10.1155/2016/2736257.
13. J.H. Hu, J.J. Cheng, S.Q. Tong, L. Zhao, J.X. Duan and Y.P. Yang, *Journal of Materials Science: Materials in Electronics*, 27 (2016) 5362.
14. X.L. Chen, N. Wu, G.W. Zhang, S.P. Feng, K.Q. Xu, W. Liu and H.B. Pan, *Int. J. Electrochem. Sci.*, 12 (2017) 593
15. Y. Suzuki, S. Pavasupree, S. Yoshikawa and R. Kawahata, *J. Mater. Res.*, 20 (2005) 1063.
16. M. Law, L.E. Greene, J.C. Johnson, R. Saykally and P.D. Yang, *Nature Mater.*, 4 (2005) 455.
17. D.V. Bavykin, J.M. Friedrich and F.C. Walsh, *Adv. Mater.*, 18 (2006) 2807.
18. H.H. Ou and S.L. Lo, *Sep. Purif. Technol.*, 58 (2007) 179.
19. D.A. Wang, B. Yu, C.W. Wang, F. Zhou and W.M. Liu, *Adv.Mater.*, 21 (2009) 1964.
20. X. Chen and S.S. Mao, *Chem.Rev.*, 107 (2007) 2891.
21. Z.D. Wei, J.G. Zhang, X.L. Song, S.Y. Ye, *New Chemical Materials*, 41 (2013) 68.
22. Z.Q. Li, H. Yang, F. Wu, J.X. Fu, L.J. Wang and W.G. Yang, *Electron. Mater. Lett.*, 13 (2017) 174.
23. S.M. Park, J.S. Yoo, *Anal. Chem.*, 21 (2003) 455.
24. G. Kresse and J. Furthmuller, *Phys. Rev. B*, 54 (1996) 11169.
25. P.E. Blochl, *Phys. Rev. B*, 50 (1994) 17953.
26. Y. Wang and J.P. Perdew, *Phys. Rev. B*, 44 (1991) 13298.
27. F. Dachille, P.Y. Simons and R. Roy, *American Mineralogist*, 53 (1968) 1929.
28. K.M.Coakley and M.D. McGehee, *Applied Physics Letters,* 83 (2003) 3380.
29. C. Goh and M.D. McGehee, *National Academy of Engineering (The Bridge)*, 35 (2005) 33.